Published in: Superconductor Science and Technology (2007), vol.20, iss. 5, pp.418-427
Status: Postprint (Author's version)

Field penetration into hard type-II superconducting tubes: effects of a cap, a non-superconducting joint, and non-uniform superconducting properties

S Denis[1,2], M Dirickx[1], Ph Vanderbemden[2], M Ausloos[3] and B Vanderheyden[2]

[1] *SUPRATECS, CISS Department, Royal Military Academy, B-1000 Brussels, Belgium*
[2] *SUPRATECS, Department of Electrical Engineering and Computer Science (B28), University of Liège, B-4000 Liège, Belgium*
[3] *SUPRATECS, Department of Physics (B5), University of Liège, B-4000 Liège, Belgium*

Abstract

Using the numerical method of Brandt (1998 *Phys. Rev.* B 58 6506), we study the penetration of a uniform magnetic field that is gradually applied parallel to the axis of finite type-II superconducting tubular samples with strong pinning. This study is carried out in view of designing low-frequency magnetic shields by exploiting the diamagnetic properties of type-II superconductors. First, we compare the field penetration into open and closed tubes. For long tubes (length larger than three times the outer diameter), we show that a cap weakly affects the maximum magnetic induction that can be shielded, but greatly increases the region over which the field is nearly uniform. When the length of the tube is shorter, both the maximum shieldable magnetic induction and the uniformity of the field attenuation are enhanced by closing the tube. We also show that making a hole in the cap, which is often necessary for applications, does not greatly affect the shielding properties provided the diameter of the hole is small compared to that of the tube (hole diameter smaller than a quarter of the outer tube diameter). In view of designing large size magnetic shields, superconducting tubes of finite size need to be joined together. We therefore examine in a second part how the presence of a non-superconducting joint between the tubes affects the shielding efficiency. It is shown that the effect of a joint depends upon its position along the tube axis and strongly increases with its size. Third, we study how non-uniform superconducting properties affect the shielding capabilities.

1. Introduction

Shielding low-frequency magnetic fields is notoriously difficult. Shields made of normal conducting materials require prohibitive thicknesses as the skin depth, δ, becomes large at low frequencies (for instance, $\delta \approx 1$ cm for copper at 50 Hz). The traditional solution of this problem consists in using a piece of ferromagnetic material instead, which can divert the magnetic flux outside the region to be protected [1]. However, hard type-II superconductors, which are strongly diamagnetic, can shield a magnetic field more efficiently than ferromagnetic materials do [2-6],

In a recent work [7], we have studied numerically and experimentally the shielding properties of open type-II superconducting tubes that were subjected to a source field applied parallel to the tube axis (parallel geometry). Three factors were considered to evaluate the quality of the shields: (i) the maximum induction that can be strongly attenuated, called B_{lim}, (ii) the spatial variation of the field attenuation, and (iii), the frequency dependence of the field attenuation. These factors were discussed in terms of two distinct routes of field penetration that are at play in an open superconducting tube. First, the applied field can penetrate by diffusing radially through the thickness of the shield, and, second, it can penetrate directly via the open ends. For a long tube, the latter mechanism is suppressed and a nearly constant attenuation results in the central region. For a given applied field, the level of this attenuation is determined by the thickness of the shield and by the magnitude of the shielding currents.

The results of [7] can be used to design better magnetic shields. For instance, putting a cap at both ends of the tube reduces the penetration from the extremities and thus raises the level of attenuation inside the tube. In practice, however, several design constraints must also be taken into account. For instance, electrical wiring is oftentimes needed to connect the inside and the outside of a magnetic shield. The wiring should be placed so that the shielding action is the least perturbed. In particular, a wiring hole is best made where the field is the weakest, which for a closed cylinder corresponds to the centre of one of the closing caps.

Other design constraints arise when considering large shields, typically of dimensions larger than a few centimetres. The type of material that can be used, and hence the quality of its superconducting properties and

the typical dimensions that can be obtained for a shield, depend on the operating temperature of the shield. If temperatures lower than 40 K are allowed by the application, magnesium diboride (MgB_2) can be used to make efficient magnetic shields [6]. The reactive liquid infiltration method allows one to realize superconducting tubes with lengths of several tens of centimetres [8, 9]. This method consists in a liquid infiltration of magnesium inside preforms of boron powders, in a closed metallic container that is heated at around 900 °C for one half to several hours. Each manufacture requires a careful design of the container and a careful distribution of the reactants. The presence of small islands of Mg_2B_{25} can cause a local reduction of the superconducting current density [8]. If the application needs temperatures higher than 77 K, high-temperature superconductors (HTSs) must be used. HTS shields may also exhibit non-uniform superconducting properties. The precursor powder always contains a small amount of impurities. The particles of the initial powder are not spherical and, as they pack on one another, the density of the obtained material can vary as a function of the position inside the material [10]. A change of density induces local variations of the critical current density, J_c. As for the preparation of MgB_2 shields, a heating step is necessary to obtain HTS materials with well connected grains. Very large superconducting shields (a few decimetres) would need very large furnaces, which could be costly. An alternative for making large type-II magnetic shields is to join smaller tubes which are heated separately.

The purpose of this paper is to extend the study of [7] to superconducting magnetic shields designed with constraints that are dictated by the applications. We consider three different illustrative systems:

(i) a tube closed with two caps, each containing a wiring hole,

(ii) an open tube made of smaller tubes that are joined with a normal material,

(iii) an open tube having non-uniform superconducting properties.

The shielding properties of these systems are studied as a function of their geometry. To our knowledge, analytical expressions of the threshold induction B_{lim}, or of the spatial variation of the field attenuation, are not available for these non-trivial geometries. We thus resort to numerical simulations. We follow Brandt's method [11], which can be easily implemented on a personal computer with standard numerical tools. A numerical study has the advantage of treating perfectly specified systems; it thus allows us to consider one effect at a time. Carrying out a similar study by experimental means is, however, much more difficult. Due to the many steps involved in fabricating large superconducting shields, many effects can cause deviations from theory. These effects often act simultaneously, which makes data interpretation arduous. Our work is meant to be a first-approximation study of the problems encountered with large superconducting shields. Being numerical, and not experimental, this approach should be taken as providing a rough guideline for the design of hard type-II magnetic shields. More work is of course required to apply this guideline for building real systems. As a reminder, we nevertheless have shown [7] that the simulations following Brandt's method reproduce the experimental data with very good accuracy for open tubes.

The report is organized as follows. In section 2, we detail the constitutive laws and set up the numerical model. Also, we briefly recall the shielding properties of an open tube in parallel geometry in section 2.3. In section 3, we present and discuss our numerical results. First, we compare the shielding properties of open and closed tubes. Second, we study how a non-superconducting ring affects the field penetration into an open tube. Third, the shielding capabilities of an open tube having non-uniform superconducting properties are presented. We conclude in section 4.

2. Theory

The numerical simulations are based on the same model and the same equations as in [7]. In this section, we recall the main hypotheses and the main equations to solve. The interested reader can find the detailed derivation in [7] and [11].

2.1. Constitutive laws

The realization of large (a few centimetres) superconducting single-grain magnetic shields is intricate and costly. Hence, as in most previous works on the fabrication of large superconducting magnetic shields [3, 6, 10, 12-18], we focus on polygrain materials [19, 20]. We assume that the shielding polycrystalline material satisfies the three following constitutive laws:

Published in: Superconductor Science and Technology (2007), vol.20, iss. 5, pp.418-427
Status: Postprint (Author's version)

$$\mathbf{B} = \mu_0 \mathbf{H}, \qquad (1)$$

$$\mathbf{E}(J) = E_c \left(\frac{J}{J_c} \right)^n \frac{\mathbf{J}}{J}, \qquad (2)$$

and

$$J_c(B) = \frac{J_{c0}}{1 + B/B_1}. \qquad (3)$$

Law (1) expresses the fact that we do not seek to describe the field penetration into individual grains but rather consider the induction B to be an average of the magnetic flux over many grains. As a result, the magnetic properties are isotropic and the material supports macroscopic shielding currents whose density is given by $J = \nabla \times B/\mu_0$. In (2), J represents the magnitude of the vector current density J, E is the electrical field and the exponent n is assumed to be independent of the local magnetic induction. This law is commonly used to model the relation *E(J)* of a type-II superconductor [11, 21, 22]. The intimate relation between flux motion and the *E(J)* relation has been recognized by many authors (see for instance [23]). For $n = 1$, the power law (2) describes an ohmic conductor, which also applies to superconductors in the regime of thermally activated flux flow at low frequencies (unpinned but damped flux lattice). In the limit $n \to \infty$, (2) is equivalent to the Bean model, and for $1 << n < \infty$, it corresponds to flux creep regimes. The third constitutive law, (3), first introduced by Kim [24], results from the polycrystalline nature of the material.

Figure 1: *Tube of internal radius a_1, external radius a_2, and length ℓ, subjected to an axial magnetic induction B_a.*

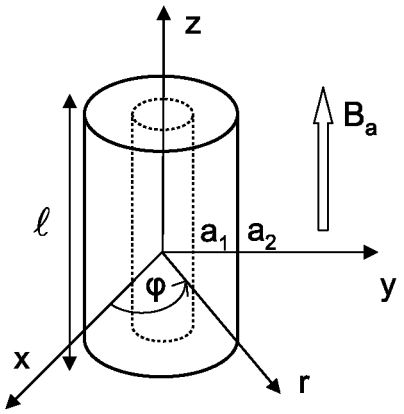

2.2. Computational method

The computational method of [7] is based on Brandt's approach [11] and is formulated for axisymmetric geometries. Consider the tube shown in figure 1 and assume an inner radius a_1, an outer radius a_2, and a length ℓ. The tube is subjected to a uniform axial magnetic induction B_a. We work in cylindrical coordinates, so that positions are denoted by *(r,φ,z)*. As the magnitude of the applied induction, B_a, is increased, the induced electric field and the resulting current density are

$$\mathbf{J} = -J(r,z)\,\hat{\varphi}, \qquad \mathbf{E} = -E(r,z)\,\hat{\varphi}, \qquad (4)$$

where φ is the unit vector in the azimuthal direction. The magnetic induction is invariant under a rotation around the z-axis and has no φ-component. Thus,

$$\mathbf{B}(r,z) = B_r(r,z)\,\hat{r} + B_z(r,z)\,\hat{z}. \qquad (5)$$

The computational method is based on the resolution of an equation of motion of the current density, J, using the Biot-Savart law discretized on a two-dimensional grid, with spatial steps Δr and Δz. Following the notations of

[7], we have

$$\dot{J}_i(t) = \frac{1}{\mu_0 \Delta r \Delta z} \sum_j Q_{ij}^{-1} \left\{ \frac{r_j}{2} \dot{B}_a - E\left[J_j(t)\right] \right\}, \qquad (6)$$

where J_i and Q_{ij} are shorthand notations for $J(\mathrm{r}_i)$ and $\mathrm{Q}(\mathrm{r}_i,\mathrm{r}_j)$, with r = ($r$,$z$). The sum in (6) only extends for points inside the superconducting volume. The kernel $Q(r,$ r') depends on the geometry of the sample. For a tubular sample which is symmetric about the plane $z = 0$ and using the notation r' = (r', z), the kernel assumes the form

$$Q(\mathbf{r}, \mathbf{r}') = f(r, r', z - z') + f(r, r', z + z'), \qquad (7)$$

with

$$f(r, r', \eta) = \int_0^{\pi} \frac{r' \cos\varphi}{2\pi \sqrt{\eta^2 + r^2 + r'^2 - 2rr' \cos\varphi}} \, \mathrm{d}\varphi. \qquad (8)$$

Imposing the initial condition

$$J_i(t = 0) = 0 \qquad \forall i, \qquad (9)$$

the current density can be numerically integrated over time by updating the relation

$$J_i(t + \Delta t) \cong J_i(t) + \dot{J}_i(t)\, \Delta t. \qquad (10)$$

2.3. Field penetration into an open superconducting tube

Before presenting our numerical results, we briefly recall the main findings of [7], concerning the field penetration in an open type-II tube in parallel geometry. These results will serve as a basis for comparison with the present results.

The sample used in [7] is a commercial HTS tube (type CST-12/80 from CAN SUPERCONDUCTORS [25]) similar to that of figure 1. It has an outer radius $a_2 = 6.5$ mm, an inner radius $a_1 = 0.8a_2$, and a length $\ell = 6a_2$. As one applies an increasing magnetic induction parallel to the z-axis, the measured internal magnetic induction at the centre follows the curve shown in figure 2 at 77 K. Simulations based on the algorithm described in section 2.2 reproduce this curve with good accuracy [7]. Below the threshold induction $B_{\mathrm{lim}} \cong 14$ mT, the internal magnetic induction remains close to zero, and strongly increases for higher applied inductions. The induction B_{lim} represents the maximum induction the sample can efficiently shield. Defining the field attenuation by

$$FA(r, z) = \frac{B_a}{B_{\mathrm{in}}(r, z)}, \qquad (11)$$

where $B_{\mathrm{in}}(r, z) = \sqrt{B_r^2(r, z) + B_z^2(r, z)}$ is the magnitude of the magnetic induction at the position (r, z) in the hollow of the tube, we adopted the convention that B_{lim} corresponds to the maximum applied induction for which the field attenuation at the centre of the tube, FA (0,0), is higher than 1000 (60 dB) :

$$\mathrm{FA}(0, 0) > 1000 \qquad \texttt{for} \quad B < B_{\mathrm{lim}}. \qquad (12)$$

The numerical results of our previous work [7] show the existence of two penetration routes into an open superconducting tube: one from the external surface of the tube, and one from the opening ends, the latter being suppressed for long tubes. These two mechanisms lead to a spatial variation of the field attenuation along the z-axis of the tube. For long tubes *($\ell > 6a_2$),* we can define a zone where the field attenuation is constant. This zone roughly extends from $z = 0$ (centre of the tube) to $|z| = \ell/2 - 3a_2$. Outside this zone, the field attenuation decreases exponentially as one moves towards the extremity of the tube. As shown in [7], B_{lim} can be approximated with good accuracy by $B_{\mathrm{lim}} \cong \mu_0 H_P$, where H_P is the field of full penetration of the superconducting tube.

For small tubes *($\ell < 6a_2$),* for which the magnetic flux penetration from the opening ends is predominant, the central zone, characterized by a constant shielding factor, is absent. In this case, it follows that $B_{\rm lim}$ is systematically smaller than $\mu_0 H_{\rm P}$. This results from the fact that the field at the centre rises rapidly with the applied field, and thus the factor FA drops below the threshold value of 60 dB well before the tube is fully penetrated. Although this case is conceptually useful for picturing the difference between $B_{\rm lim}$ and $\mu_0 H_{\rm P}$, the interest of using short open type-II tubes for magnetic shielding applications is very limited.

Figure 2: *Evolution of the internal magnetic induction at the centre of an open tube as a function of the applied magnetic induction for the sample considered in [7]. The tube has an external radius a_2, an internal radius $0.8a_2$, and a length $\ell = 6a_2$.*

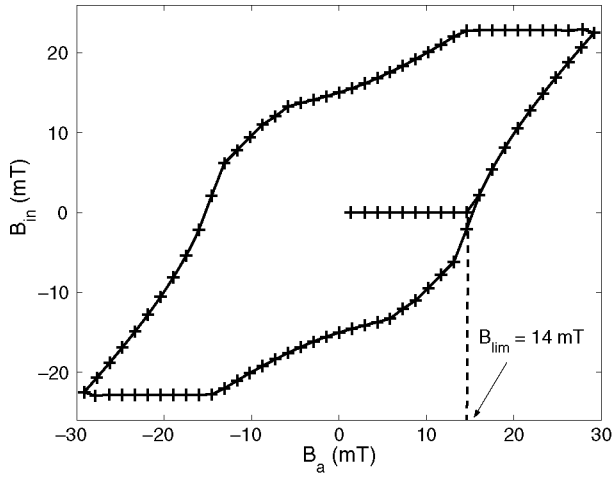

2.4. Model parameters

In [7], the parameters J_{c0} and B_1 entering the constitutive laws (3) were determined by fitting the curve of first magnetization of figure 2 to an analytical expression obtained from Maxwell's equations and Kim's model [24], while the exponent n in (2) was obtained from an analysis of the frequency dependence of the field attenuation at the centre (r = 0, z = 0) of the sample. These procedures lead to the values [7]

$$n = 25, \qquad (13)$$

$$J_{c0} = 1782 \text{ A cm}^{-2}, \qquad (14)$$

$$B_1 = 5 \text{ mT}. \qquad (15)$$

Although the results of this paper will not be compared to experimental data, we use the same values, determined at 77 K, in order to take realistic parameters. A higher J_{c0} leads to a higher $B_{\rm lim}$ for long tubes. We further assume that the external magnetic induction is varied with a constant sweep rate given bv

$$\dot{B}_{\rm a} = \pm E_{\rm c}/a_2 \cong \pm 12.5 \text{ mT s}^{-1}. \qquad (16)$$

The plus (minus) sign corresponds to increasing (decreasing) applied inductions. This temporal evolution allows one to follow the full hysteretic curve of the superconducting shield. Results corresponding to faster or slower temporal ramps can be directly obtained from the results we present here by applying the scaling laws described in [7, 11],

3. Numerical results and discussions

3.1. Field attenuation for open and closed tubes

Closed tubes should present better shielding properties than open tubes, as one expects the penetration from the extremities to be reduced in the presence of a cap. However, allowing an electrical connection between the inside and the outside of a shield is always necessary. In this section, we compare the shielding properties of the three following systems:

- system 1: an open tube (figure 3(a));
- system 2: a tube closed by caps (figure 3(b));
- system 3: a tube closed by caps, each pierced by a hole (figure 3(c)).

The three systems are depicted in figure 3. For symmetry reasons, only a quarter of each system is shown.

The three systems are subjected to an axial induction of magnitude B_a, which increases at a constant rate $\dot{B}_a = E_c/a_2$. We consider tubes with dimensions similar to that in [7], with $a_2 = 8$ mm, $a_1 = 6.5$ mm, and thus a thickness $d = a_2 - a_1 = 0.2a_2 = 1.5$ mm. The thickness of the cap and the radius of the holes of sample 3 are also chosen equal to $d = 0.2a_2$. These represent realistic values, both for the thicknesses that can be practically obtained, for instance by isostatic pressing methods as in [25], and for the radius of the hole that is necessary for housing an electrical connection.

We first compare the threshold induction B_{lim} of the three systems as a function of the length ℓ. Afterwards, we compare the uniformity of the field attenuation realized by the three systems.

3.1.1. The threshold induction B_{lim}.

Table 1 gives the values of B_{lim} for the three systems and for different values of the ratio ℓ/a_2. One can notice that, for short open tubes, with $\ell/a_2 \leq 2$, the field attenuation at the centre is lower than 60 dB for all inductions. It is therefore not possible, according to (12), to determine B_{lim} in these cases. In the range of ratios $2 \leq \ell/a_2 \leq 6$, the threshold induction can be defined, and it is found to be systematically higher for the closed tube than for the open one. For $\ell = 3a_2$, the value of B_{lim} for the closed tube is twice as large as that for the open tube. For ratios larger than $\ell = 5a_2$, the parameters B_{lim} for the three systems differ by less than 1.5%. Note also that as soon as $\ell/a_2 \geq 3$, the threshold induction B_{lim} for sample 3 is not significantly different from that for sample 2. This can be easily understood, as for these ratios, the shielding attenuation at the centre is less affected by the penetration via the openings [7] and thus a wiring hole has limited effects.

Figure 3: *(a) system 1: open tube of length ℓ, with a wall thickness $d = a_2 - a_1 = 0.2a_2$; (b) system 2: closed tube with a cap of thickness $d = 0.2a_2$; (c) system 3: closed tube with a hole in the cap; the radius of the hole is $d = 0.2a_2$. For each sample, the induction is applied along the z-axis. Only a quarter of each system is shown for symmetry reasons.*

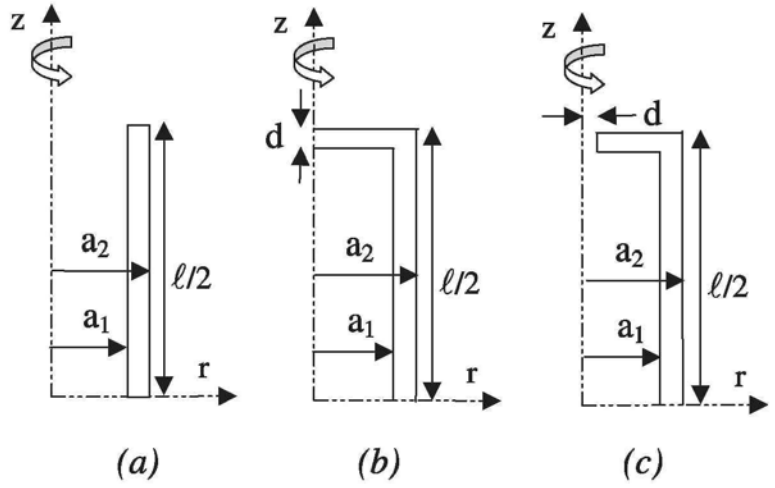

Figure 4 shows the evolution of the internal magnetic induction as a function of the applied induction for the three systems, when $\ell = 3a_2$. The inset shows the range of inductions below threshold, $B_a < B_{lim}$. We see that the global evolution of the magnetic induction at the centre of the tube is not significantly affected by the cap. In the inset, one can also see that, at low applied inductions, the internal induction, B_{in}, is systematically higher in system 1 (open tube) than in the two other systems.

Figure 4: *Evolution of the internal magnetic induction (at the centre) as a function of the applied induction for the three systems depicted in figure 3 and for a ratio $\ell/a_2 = 3$.*

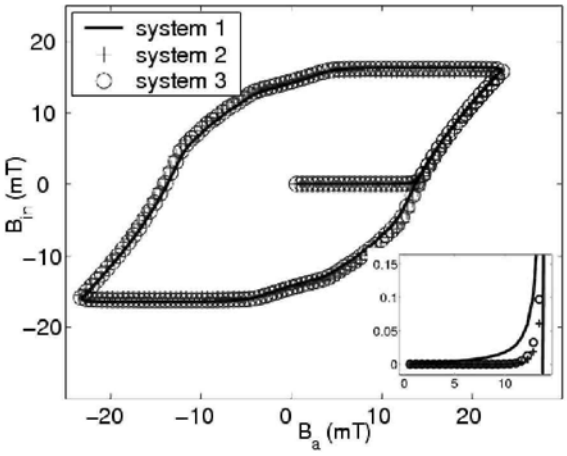

Table 1: *Comparison of the threshold induction B_{lim} (in mT) for the three systems of figure 3 and for different ratios ℓ/a_2.*

ℓ/a_2	System 1	System 2	System 3
1	—	10.69	9.72
2	—	11.66	10.69
3	6.41	12.63	12.25
4	12.83	13.41	13.22
5	13.61	13.80	13.80
6	14	14	14
7	14	14	14
8	14	14	14

Figure 5: *Magnetic field lines for systems 1, 2, and 3 if $B_a = 0.8B_{lim}$. The field lines distribution is weakly (resp. significantly) affected by the hole of system 3 in the region delimited by the dashed circle (resp. square).*

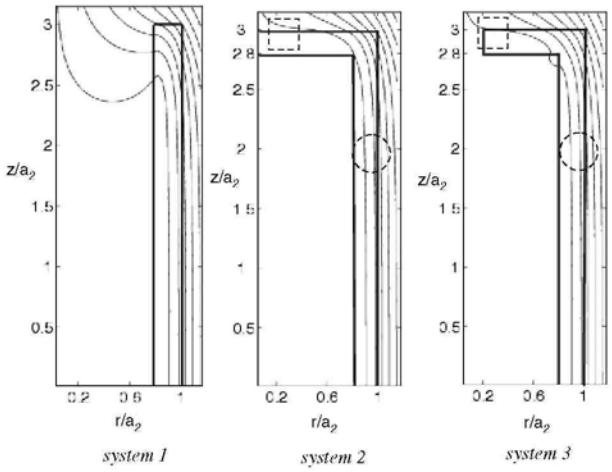

3.1.2. The spatial variation of the field attenuation.

We saw in the previous section that for long tubes, with an aspect ratio $\ell/a_2 \geq 6$, adding a cap does not significantly increase the threshold induction B_{lim}. We now turn to studying the effect of adding a cap to long tubes ($\ell = 6a_2$ in this case) on the spatial variation of the field attenuation, and comparing systems 1 (no cap) and 2 (two caps). Afterwards, we compare systems 2 and 3.

Figure 5 shows the magnetic field lines for the three systems, assuming a magnetic induction $B_a = 0.8B_{lim}$ applied after zero-field cooling. For symmetry reasons, only a quarter of each system is shown. Figure 6 shows the contour lines of the ratio between the FA for system 2 and for system 1, when $B_a = 0.8B_{lim}$.

From figure 5, a difference in the flux line patterns can be clearly observed between system 1 and system 2. In the latter case, the shape of the field lines is close to that of a bulk cylinder, which at this induction would only be partially penetrated through its outer surface [7, 11, 26]. For the central region, $z/\alpha_2 < 1$, and for both systems 1 and 2, the internal magnetic induction is mainly due to the penetration through the thickness of the tube and not through the opening ends. Thus, the cap does not significantly affect the attenuation factor, which explains why the gain plotted in figure 6 is smaller than ~3 in this region. For larger values of z, the penetration from the opening ends is the main penetration mechanism for system 1, whereas this mechanism is strongly reduced in system 2. Therefore, the gain plotted in figure 6 increases as one moves towards the extremity. This can also be seen more clearly in figure 7, which shows the field attenuation obtained along the z-axis in the three systems, and for $B_a = 0.8B_{lim}$. The field attenuation decreases by a factor of ~10 (20 dB) between Z = 0 and 2.5 for the closed tube (system 2), whereas it decreases by a factor ~1000 (60 dB) for the open tube (system 1). Near the extremities and close to the internal surface, $z = 2.5$, $r = a_1$, we observe in figure 5 a concentration of the magnetic field lines due to the finite length of sample 2. Accordingly, the gain in field attenuation in figure 6 is reduced in this region (lower than 20 dB). Note that the contour lines of figure 6 are not parallel to the r-axis and that the cap effects vary greatly inside the tube. The non-penetrated central part of the cap of system 2 repels the field lines from the z-axis. Hence, the difference between the field lines distribution of systems 1 and 2 is stronger near the axis than near the internal surface, $r = a_1$. Finally, the ratio of the FA of systems 2 and 1 increases as one moves towards r = 0.

To express these findings quantitatively, let us define an effective volume, V_{eff}, as the volume over which the local values of the field attenuation are at most 5 dB lower than the field attenuation at the centre (z = 0 and r = 0). From the values of FA given above, we find V_{eff} =1.67 cm^3 for system 1 and V_{eff} = 2.08 cm^3 for system 2. Thus, even though B_{lim} is similar in both systems, a cap increases V_{eff} by about 25%, which is a substantial gain in the quality of the shield.

If we now look at the volume where the FA of system 2 (closed tube) is higher by 5 dB than the FA of system 1 (open tube), we have found that this volume decreases as the applied induction increases: this volume is respectively equal to 4.17, 3.62, and 3.16 cm^3 for $B_a = 0.7$, 0.8, and $0.9B_{lim}$. This follows from the fact that as the applied induction increases, the field starts penetrating through the cap. So, the benefit of using a cap is useful mostly for low applied fields.

We now turn to the differences of the shielding properties between system 2 and system 3. Figure 8 shows the contour lines of the ratio of the FA for system 3 over that of system 2, and for an applied induction $B_a = 0.8B_{lim}$. Due to the presence of the hole, the FA of system 3 is reduced near the extremity and close to the axis, $z/a_2 = 2.5$, $r/a_2 = 0$. This reduction, by a factor ~10 (20 dB), is only found in the vicinity of the hole. This can also be seen in figure 7, where the curve corresponding to system 3 shows a kink in the vicinity of the hole. For positions with $z/a_2 < 2.5$, the FA of system 3 is smaller than that of system 2, though roughly of the same order of magnitude. The effective volume, V_{eff}, is respectively equal to 2.08 and 2.02 cm^3 for systems 2 and 3 if $B_a = 0.8B_{lim}$.

Figure 6: *Contour lines of the ratio of the field attenuation realized by system 2 over that realized by system 1, for $B_a = 0.8B_{lim}$*

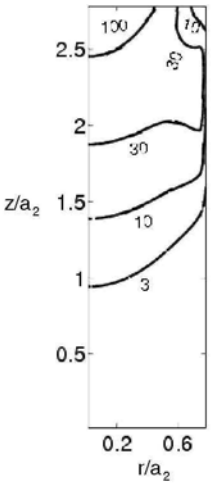

Figure 7: *Field attenuation FA for systems 1, 2, and 3 along the Z-axis, for $B_a = 0.8B_{lim}$. As a reminder, B_{lim} is nearly the same for the three samples, as $\ell = 6a_2$.*

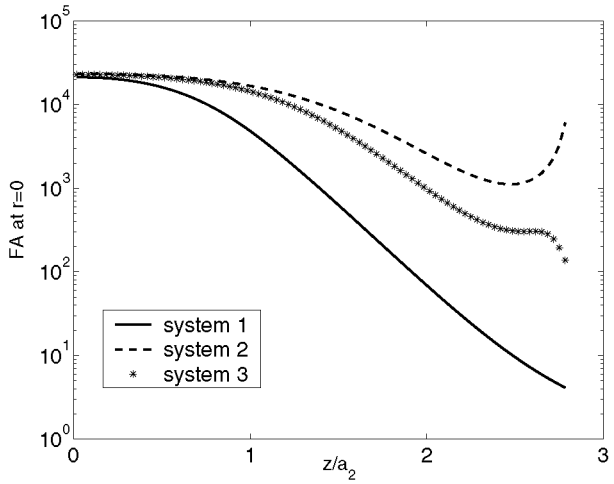

Figure 8: *Contour lines of the ratio of the field attenuation realized by system 3 over that realized by system 2. The applied induction is $B_a = 0.8B_{lim}$.*

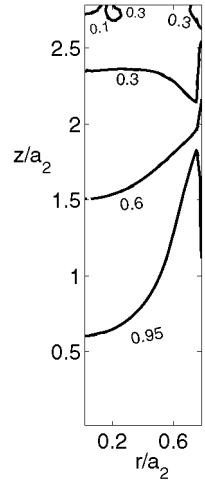

One may wonder how the size of the hole in system 3 modifies the shielding properties. When the radius of the hole is reduced by a factor 2, V_{eff} is equal to 2.06 cm^3, and the FA increases by about 14 dB near r = 0, z = *t/2*. In contrast, V_{eff} is reduced respectively to 1.78 and 1.52 cm^3 when the hole radius is doubled (hole radius equal to $0.4\alpha_2$) or tripled (giving a radius of $0.6a_2$). In the latter case, the FA is reduced by a factor of ~40 dB near z = *ℓ/2*. This suggests that the smallest possible apertures should be used when designing a superconducting magnetic shield.

From figure 8, we see that the effect of a hole is more important near the z-axis, directly below the hole, than near the inner surface at r = a_1. Indeed, the contour lines of figure 8 are not parallel to the r-axis. Consider the field lines distribution of figure 5. In the region near $r = a_1$, delimited by dashed circles, the field lines are not significantly different for system 3 and system 2. By contrast, we observe a deeper penetration in the zone delimited by a dashed square near the z-axis for system 3. Hence, the difference between the shielding properties of systems 2 and 3 is stronger in this region. For applied inductions higher than $0.8B_{\text{lim}}$, the central part of the cap of system 2 becomes penetrated, reducing its effect on the shielding properties. Hence, the difference between the shielding properties of systems 2 and 3 decreases as the applied induction increases.

3.2. Tube presenting an annular defect

As already mentioned in the introduction, the realization of efficient large superconducting shields is a technical challenge. One possibility to make large superconducting magnetic shields would be to join different tubes together after the heating process, to obtain a larger one. In this section, we study the effect of a non-superconducting joint on the shielding properties. This study can also be used as a rough model for the effects of local defects, which in this case are assumed to have an annular shape.

Figure 9 shows the geometry used for the simulations. Here, we are no longer assuming that the tube is symmetric about the plane $z = 0$. A superconducting tube with length $\ell = 8\alpha_2$ and inner radius $a_1 = 0.8\alpha_2$ contains a non-superconducting ring of thickness $e = a_2/30$ at $z = h$ (black rectangle). The applied field is supposed to be quasistatic, whence we can neglect the induced currents within the normal joint with respect to superconducting shielding currents. Due to the presence of the junction, we expect the FA to be depressed in the hollow of the superconducting tube. In this section, we evaluate this reduction and the volume of influence of the non-superconducting joint as a function of its position, *h*.

Figure 10 shows the contour lines of the relative field attenuation, RFA, which is defined as

$$\text{RFA} = \frac{\text{FA(tube with a joint)}}{\text{FA(tube without a joint)}}, \qquad (17)$$

for an applied induction $B_a = 0.8B_{\text{lim}}$ and a joint that is located at equal distance from both ends, $h = 0$. Here, B_{lim} is evaluated for a tube without the joint. Figure 11 shows the same ratio RFA at $B_a = 0.8B_{\text{lim}}$, but along the z-axis (r = 0), and for different positions *h* of the joint. From figure 10, we see that the joint not only reduces the FA in its neighbourhood, where $r \sim a_1 = 0.8a_2$, but also in a region extending all the way to the tube axis, at r = 0. Along the axis, the RFA is significantly smaller than 1 (0dB) for $|z|/\alpha_2 < 1.5$ and reaches 0.2 (-14 dB) at the centre, $r = 0$ and $z = 0$. The maximum reduction of FA and the volume of the zone of influence of the joint decrease as the position *h* of the joint increases. The position of the minimum of the RFA, z_{min}, roughly coincides with the position of the joint as long as $h/a_2 \leq 1$. For larger values of *h*, z_{min} is pushed away from the joint towards the middle of the tube, $z_{\text{min}} < h$ (see figure 11).

The behaviour of the location of the minimum of the RFA as a function of the position *h* of the defect can be explained as follows. When the joint is located near the tube extremity, $z = \ell/2$, the penetration via the openings is enhanced by the presence of the joint, while the radial penetration through the cylindrical shell is unchanged over most of the length ℓ of the tube. This affects the balance between the two penetration routes in favour of that occurring via the ends. As a result, the RFA minimum locates at lower *z*-values than the position of the joint.

In a tube without a joint, the parts located near $z = \ell/2$ are first penetrated due to demagnetizing effects [7]. Hence, the effect of a joint is smaller if the joint is located near $z = \ell/2$ than if it is located at the middle, $z = 0$ (see figure 11). We have also found that the RFA increases with the applied induction (not shown here). Indeed, as the applied induction increases, the part of the tube being fully penetrated increases in size, reducing the effect of the joint. Therefore, the effect of the joint is stronger at low applied fields.

Figure 9: *Tube with an annular defect or a non-superconducting joint of thickness $e = a_2/30$, located at $z = h$.*

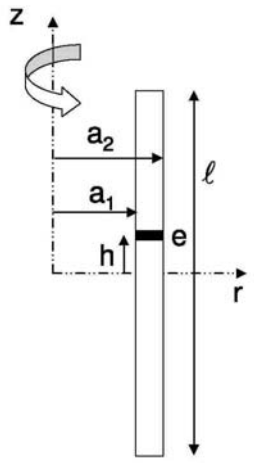

Figure 10: *Contour lines of the ratio between the FA of a tube with an annular joint and that of a tube without a joint (see (17)). The applied induction is $B_a = 0.8B_{lim}$, where B_{lim} is defined as the threshold induction for the tube without the joint.*

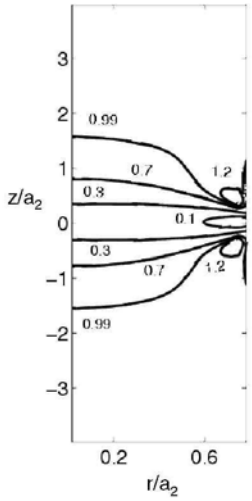

Figure 11: *Variation of the ratio RFA, (17), along the z-axis and for different positions of the joint. The applied induction is $B_a = 0.8B_{lim}$.*

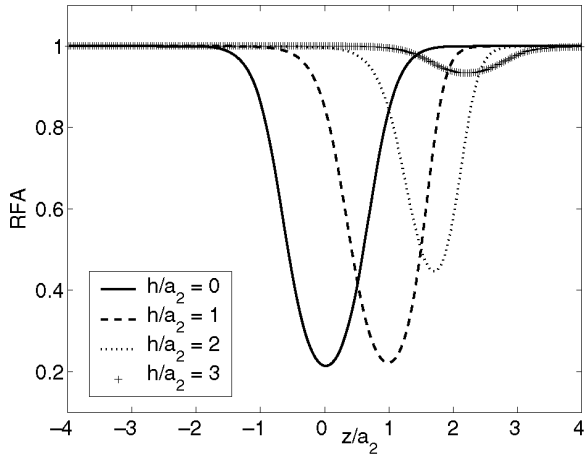

In figure 10, we observe some regions near the weld where the RFA is higher than 1. This has to be related to the negative B_z component near the extremities of an open superconducting tube subjected to an axial field [7]. Due to end effects, there is a concentration of the counter magnetic field lines near the joint, which locally enhances the shielding properties of the tube.

Figure 12 shows the FA along z at r = 0 for different thicknesses e of the weld. As the thickness of the joint e increases, the spatial variation of the reduction of the field attenuation still exhibits the shape shown in figure 10. But both the width of the region where FA is reduced and the amplitude of its reduction increase with e.

Whereas the FA is reduced by 14 dB when the thickness of the weld is $a_2/30$, it is decreased by 40 dB when the thickness e is multiplied by 3 ($e = a_2/10$)! In figure 12, we also see that the region over which the FA is significantly reduced grows as the thickness of the weld increases. So, for practical considerations, it is important to have a joint that is as small as possible.

In the last part of this section, we present two possibilities to reduce the effect of the non-superconducting joint as illustrated in figure 13. Here, the joint is located at $h = 0$ and its thickness e is equal to $a_2/30$. The first possibility is to enclose the joint with a superconducting ring (figure 13(a)). The height of the ring is $t = 3\ e$ and its width is $d = 0.2a_2 = a_2 - a_1$. The second possibility is to make a sleeve as illustrated in figure 13(b). Depending on the fabrication process, several sleeve shapes are possible. As a first approach, we consider the geometry of figure 13(b) to simplify the calculations.

Figure 12: *Field attenuation along the z-axis for different values e of the joint thickness. The field attenuation without a joint is also shown for comparison. The applied induction is* $B_a = 0.8B_{lim}$.

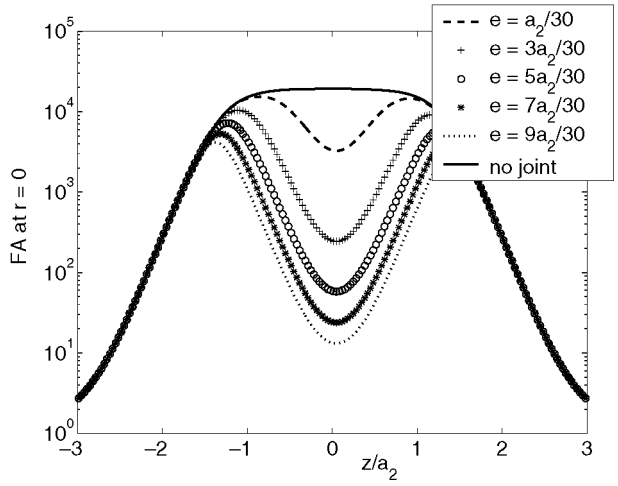

Figure 13: *Two possibilities to reduce the effect of the non-superconducting joint. The thickness e is* $a_2/30$ *and* $t = 3e$.

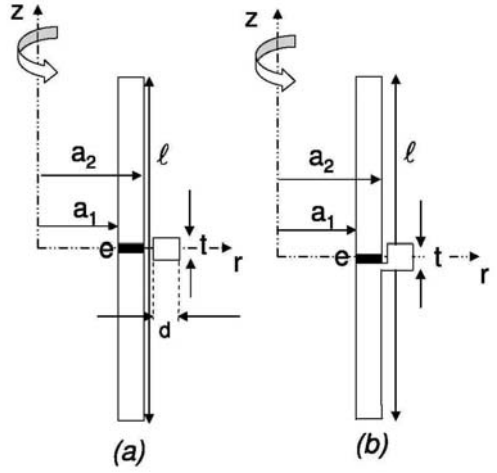

Figure 14 shows the field attenuation along the z-axis for a tube without a joint, for a tube with a joint, and finally, for the solutions (a) and (b) of figure 13. The inset is an enlargement for $|z/a_2| < 2$. There is still an entry for the magnetic flux for the two proposed solutions, and so we do not recover the field attenuation of a tube without the annular defect. Nevertheless, the field attenuation is higher when using one of the two solutions of figure 13, in particular in the central region for which $|z/a_2| < 1$. At the centre $z = r = 0$, the FA is increased by 9 dB when adopting solution (a). The field attenuation realized by systems (a) and (b) of figure 13 is nearly the same, although slightly higher for system (a) (2 dB higher at $z = r = 0$). We can also see that the maximum of the FA is no longer located at the middle of the tube, $z = 0$, due to the joint.

Figure 14: *FA along the z-axis for the two solutions of figure 13, for a tube without a joint, and for a tube with a joint. The applied induction is $B_a = 0.8B_{lim}$, where B_{lim} is the threshold induction for a tube without a joint. The inset is a enlargement near $z = 0$.*

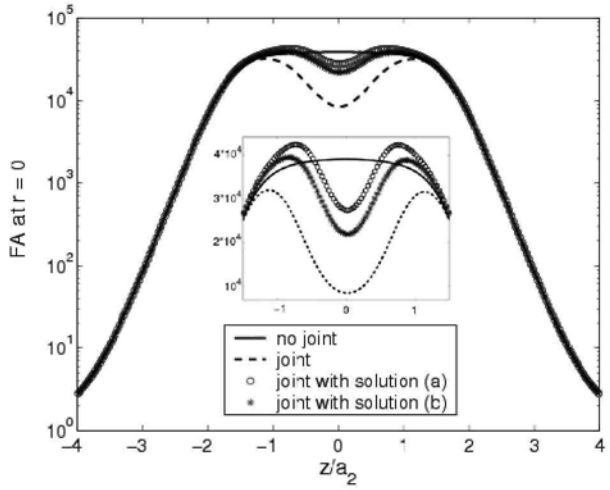

3.3. Effect of inhomogeneities on the shielding properties

As mentioned in the introduction, the realization of large superconducting shields presenting uniform superconducting properties is not obvious. Several parameters can alter this uniformity during both the fabrication and the heating process. In parallel geometry, when a hard type-II tube presents uniform superconducting properties along the z-axis, the maximum field attenuation is obtained at the centre of the tube [7]. Here, we study the change of position of this maximum when the tube has non-uniform superconducting properties. More specifically, we consider a case in which the tube presents two different values of the J_{c0} parameter entering (3). We consider the system of figure 15 which, for $z < \ell/4$, exhibits a current density with $J_{c0} = 0.8 \times 1782$ A cm^{-2} $\cong$ 1425 A cm^{-2}, and for $\ell/4 < z < \ell/2$, has $J_{c0} = 1782$ A cm^{-2}. The tube has an internal radius $a_1 = 0.8\alpha_2$ and a length $\ell = 8\alpha_2$

Figure 16 shows the variation of the field attenuation along the z-axis for different applied inductions. Here, B_{lim} is 12 mT. From figure 16, we see that the maximum field attenuation occurs at the centre of the tube ($z = 0$) when $B_a = 0.80B_{\text{lim}}$. As the applied induction is further increased, this position moves towards higher z-values and lies near $z = 2a_2$, i.e. the position of the boundary between the two parts of the tube with different J_{c0}-values. Hence, the position of the maximum field attenuation depends upon the magnitude of the applied induction when the tube has non-uniform superconducting properties.

For low B_a-values, the tube is only partly penetrated along its side wall and some field can penetrate from the opening end at $z = \ell/2$. This results in a field attenuation that is maximum at the centre of the tube. As B_a is increased, the lower part, $Z < \ell/4$, is penetrated before the upper part, $z > \ell/4$, because of the lower J_{c0}-value. Therefore, the magnetic field can fully penetrate for $z < \ell/4$, reducing the field attenuation there. As some parts of the tube are not fully penetrated for $z > \ell/4$, the maximum of the field attenuation lies in this region. As B_a is further increased, the part with the lower J_{c0}-value no longer acts as a shield. The magnetic field can then penetrate from the region $z < \ell/4$ towards higher z-values, by the same route which allows the flux to penetrate via the ends of an open tube. As a result, the maximum field attenuation position moves towards larger z.

Figure 15: *System used to study the effect of non-uniform superconducting properties on the field attenuation. The tube has an internal radius equal to $a_1 = 0.8a_2$, and a length $\ell = 8a_2$. The tube has two different values of J_{c0}, depending the position along the z-axis. For $z < \ell/4$, $J_{c0} = 1425$ A cm^{-2}; for $\ell/4 < z < \ell/2$, $J_{c0} = 1782$ A cm^{-2}.*

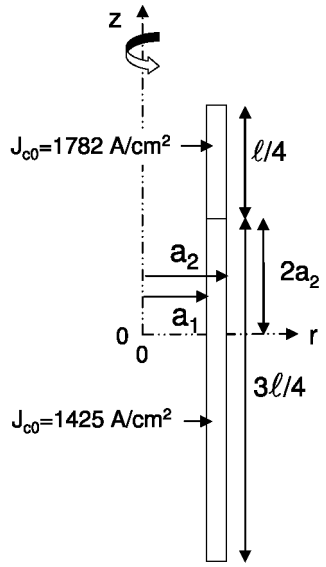

Figure 16: *Field attenuation along the z-axis (r = 0) at different applied inductions, for the system described in figure 15 having non-uniform superconducting properties.*

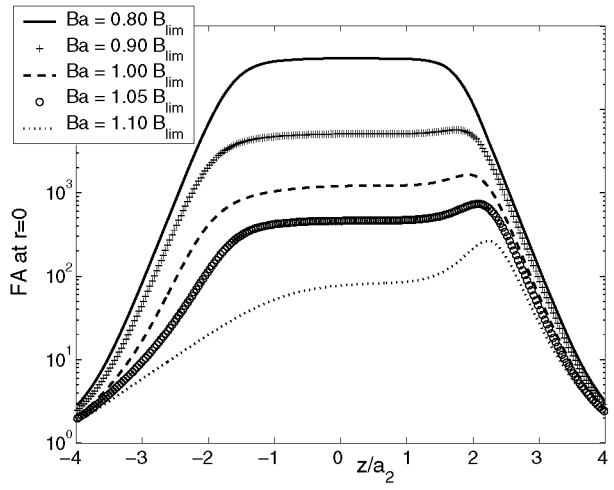

4. Conclusions

We have calculated the shielding properties of tubular hard type-II superconducting samples with features of practical interest, subjected to an axial field. The numerical simulations are based on the algorithm described in [11]. This study was carried out in view of designing efficient superconducting magnetic shields. Our results can be summarized as follows.

For long tubes, $\ell > 6a_2$ (where ℓ is the tube length and a_2 is the external radius), a cap does not increase the maximum shieldable magnetic induction B_{lim}, but reduces the spatial variation of the field attenuation. A closed tube thus presents a larger volume with a field attenuation higher than a given level. For small tube lengths, $\ell < 6a_2$, closed tubes also present more uniform shielding properties than open tubes. In addition, the threshold induction B_{lim} is higher for closed tubes if $\ell < 6a_2$, as the importance of the penetration route from the extremities is reduced by the cap. Hence, using closed tubes is particularly interesting when the volume to shield is small. As a connection is always needed between the inside and the outside of a shield, one must also consider holes in the cap. A small hole, of diameter equal to a quarter of the cap diameter, weakly reduces the shielding capabilities of closed tubes. In contrast, large holes, with a diameter larger than the half of the cap diameter, drastically reduce

the shielding properties. Hence, the size of the apertures has to be minimized for shielding applications.

The introduction of a non-superconducting joint between stacked tubes reduces the field attenuation all along the diameter of the tube, and not only in a small region around the weld. The reduction is higher if the joint is located near the centre of the tube. Nevertheless, the effect of this non-superconducting part is relatively weak if the joint is thin. Hence, care must be taken to have the thinnest possible weld when joining different tubes to obtain a larger one. Covering the soldering by a superconducting ring or using a sleeve strongly reduces the effect of the joint.

When an open superconducting tube has uniform superconducting properties, the field attenuation is maximum at the centre of the tube. This is no longer the case when the tube presents non-homogeneities. In particular, the position of this maximum depends upon the magnitude of the applied magnetic induction.

Acknowledgments

This research was supported in part by a ULg grant (Conseil de la Recherche support through project 'Fonds spéciaux' (C-06/03)) and by the Belgian FNRS (grant from FRFC: 1.5.115.03). We also thank the Royal Military Academy (RMA) of Belgium for equipment grants.

References

[1] Clayton R P 1992 *Introduction to Electromagnetic Compatibility* (New York: Wiley)

[2] Pavese F 1998 Magnetic shielding *Handbook of Applied Superconductivity* (Bristol: Institute of Physics Publishing) pp 1461-83

[3] Grenci G, Denis S, Dusoulier L, Pavese F and Penazzi N 2006 *Supercond. Sci. Technol.* 19 249-55

[4] Mager A J 1970 *IEEE Trans. Magn.* 6 67-75

[5] Shenfeld S 1968 *IEEE Trans. Electromagn. Compat.* 10 29-34

[6] Cavallin T, Quarantiello R, Matrone A and Giunchi G 2006 *J. Phys. Conf. Ser.* 43 1015-8

[7] Denis S, Dusoulier L, Dirickx M, Vanderbemden Ph, Cloots R, Ausloos M and Vanderheyden B 2007 *Supercond. Sci. Technol.* 20 192-201

[8] Giunchi G, Ripamonti G, Cavallin T and Bassani E 2006 *Cryogenics* 46 237-42

[9] Giunchi G, Ceresara S, Ripamonti G, Chiarelli S and Spadoni M 2003 *IEEE Trans. Appl. Supercond.* 13 3060-3

[10] Dusoulier L *et al* 2006 *Key Eng. Mater.* 314 153-7

[11] Brandt E H 1998 *Phys. Rev.* B 58 6506-22

[12] Omura A, Oka M, Mori K and Itoh M 2003 *Physica* C 386 506-11

[13] Pavese F, Bianco M, Andreone D, Cresta R and Rellecati P 1993 *Physica* C 204 1-7

[14] Plechacek V, Hejtmanek J, Sedmidubsky D, Knizek K, Pollert E, Janu Z and Tichy R 1995 *IEEE Trans. Appl. Supercond.* 5 528-31

[15] Matsuba H, Yahara H and Irisawa D 1992 *Supercond. Sci. Technol.* 5 S432-9

[16] Plechacek V, Pollert E and Hejtmanek J 1996 *Mater. Chem. Phys.* 43 95-8

[17] Pavese F, Bergadano E, Bianco M, Ferri D, Giraudi D and Vanolo M 1996 *Adv. Cryog. Eng.* 42 917-22

[18] Omura A, Kotani K, Yasu K and Itoh M 2006 *J. Phys. Chem. Solids* 67 43-6

[19] Vanderbemden Ph, Destombes Ch, Cloots R and Ausloos M 1998 *Supercond. Sci. Technol.* 11 94-100

[20] Doyle R, Bradley A, Lo W, Cardwell D, Campbell A M, Vanderbemden Ph and Cloots R 1998 *Appl. Phys. Lett.* 73 117-20

[21] Brandt E H 1996 *Phys. Rev.* B 54 4246-64

[22] Brandt E H 1995 *Rep. Prog. Phys.* 58 1465-594

[23] Yeshurun Y, Malozemoff A P and Shaulov A 1996 *Rev. Mod. Phys.* 68 911-49

[24] Kim Y B, Hempstead C F and Strnad A R 1962 *Phys. Rev. Lett.* 9 306-9

[25] http://www.can.cz/shields.php

[26] Navau C, Sanchez A, Pardo E, Chen D-X, Bartolom E, Granados X, Puig T and Obradors X 2005 *Phys. Rev.* B71 214507-1-9